Resolving the dynamic structure of chlorosomes in green sulfur bacteria by MAS NMR

Dsouza, L.A.

Appendix

Appendix 1: Supporting information for Chapter 2

An Integrated Approach Towards Extracting Structural Characteristics of Chlorosomes from a *bchQ* Mutant of *Chlorobaculum tepidum*

Table S2.1 ^{13}C chemical shifts for chlorosomes of *bchQ* from *Cba. tepidum* in ppm: liquid σ_{liq}^{C}, solid-state σ_{s}^{C} and aggregation shifts $\Delta\sigma_{s}^{C} = \sigma_{s}^{C} - \sigma_{liq}^{C}$

Position	σ_{liq}^{C} (Balaban *et al*. 1995)[1]	σ_{s}^{C} chlorosomes	$\Delta\sigma_{s}^{C}$ chlorosomes
1-C	153.79	154.1	0.3
2-C	135.08	134.9	-0.2
3-C	145.13	139.0	-6.2
4(I)-C	145.37	145.3	-0.1
4(II)-C		144.1	
5(I)-CH	100.03	96.0	-4.1
5(II)-CH		102.3	
6(I)-C	150.72	150.8	0.1
6(II)-C		150.5	
7(I)-C	133.45	130.2	-3.2
7(II)-C		131.7	
8-C	143.39	143.7	0.3
9-C	146.01	147.3	1.2
10-CH	105.57	106.4	0.8
11-C	146.47	147.4	0.9
12-C	140.65	140.6	-0.1
13-C	130.26	130.5	0.2
14-C	161.24	161.8	0.6
15-C	104.74	104.3	-0.4
16-C	153.98	154.5	0.5
17-CH	50.07	50.0	0.0

18-CH	47.64	48.3	0.6
19(I)-C	167.76	171.0	3.2
19(II)-C		168.2	
20(I)-C	104.74	105.6	0.9
20(II)-C		103.9	
2^1-CH_3	16.76	14.4	-2.3
3^1(I)-CH	64.95	63.9	-1.1
3^1(II)-CH		63.7	
3^2(I)-CH_3	25.43	22.3	-3.1
3^2(II)-CH_3		25.4	
7^1(I)-CH_3	10.37	6.2	-4.1
7^1(II)-CH_3		11.2	
8^1-CH_2	19.14	19.9	0.7
8^2-CH3	16.97	19.9	2.9
12^1-CH_2	20.77	18.4	-2.4
12^2-CH_3	16.56	18.4	1.9
13^1(I)-C	197.49	196.2	-1.3
13^1(II)-C			
13^2-CH_2	48.28	48.7	0.4
17^1-CH_2	29.6	29.9	0.3
17^2-CH_2	30.6	29.9	-0.7
17^3-C	173.62	173.2	-0.5
18^1-CH	20.36	21.4	1.0
20^1-CH_3	20.96	21.5	0.5
F1-CH_2	61.14		
F2-CH	117.5		
F3-C	142.23	140.9	-1.3
F4-CH_2	39.22		
F5-CH_2	26.23	26.2	0.0
F6-CH	123.19	123.9	0.7
F7-C	134.98		
F8-CH_2	39.02	39.6	0.5
F9-CH_2	25.7	24.9	-0.8

F10-CH	123.87		
F11-C	130.82		
F12-CH_3	25.04		
F3^1-CH_3	15.79	16.1	0.3
F7^1-CH_3	15.35		
F11^1-CH_3	17.03		

*I and II correspond to two components present in the system. A lower in chemical shift value is considered as component (I) and which has a higher chemical shift value is considered component (II)

**Blank space indicates that no chemical shift values could be derived from the experiment.

***Aggregation shifts that is > |1.5| ppm is seen for carbon resonances such as 3-C, 5-C, 7-C, 19-C, 2^1-C, 3^2-C, 7^1-C, 8^2-C, 12^1-C, 12^2-C, 13^1-C, F3-C. These mostly originate from rings 1 and 3.

Table S2.2 ^{1}H chemical shifts for chlorosomes of *bchQ* from *Cba. tepidum* in ppm: liquid σ_{liq}^H, solid-state σ_s^H and aggregation shifts $\Delta\sigma_s^H = \sigma_s^H - \sigma_{liq}^H$.

Position	σ_{liq}^H(van Rossum *et al*. 2001)[2]	σ_s^H chlorosomes	$\Delta\sigma_s^H$ chlorosomes
2^1 (I) - H_3	3.3	0.7	-2.6
2^1 (II) - H_3		1.4	
3^1(I)- H	6.25	3.4	-2.8
3^1(II) - H			
3^2(I) - H_3	2.01	1.1	-0.9
3^2(II) - H_3			
5(I) - H	9.56	6.9	-2.7
5(II) - H	9.56	7.4	-2.1
7^1(I) - H_3	3.19	-0.7	-3.9
7^1(II) - H_3	3.19	3.3	0.1
8^1 - H_2	3.67	1.0	-2.7
8^2 - H_3	1.62		
10 - H	9.43	9.8	0.4

12^1 - H_2	3.97	2.4	-1.6
12^2 - H_3	1.79		
13^2 - H_2	5.09	5.0*	-0.1
17 - H	4.08	4.8	0.7
17^1 - H_2	2.00/2.20	2.1	0.1/-0.1
17^2 - H_2	2.35/2.42	2.1	-0.2/-0.3
18(I) - H	4.52	5.0*	0.5
18(II)- H	4.52		-4.5
18^1(I) - H_3	1.43	3.8*	0.1
18^1(II) - H_3	1.43		-1.4
20^1 - H_3	3.72	3.8*	
F1 - H_2	4.31	4.0	-0.3
F2 - H	5.05	6.8	1.7
F4 - H_2	1.88	2.9	1.0
F5 - H_2	1.88		
F6 - H	4.95		
$F7^1$- H_3	1.5		
F8 - H_2	1.88	1.6	-0.3
F9 - H_2	1.88		
F10 - H	4.95		
$F11^1$ - H_3	1.5		
F12 - H_3	1.54	1.4	-0.1

Asterisk (*) indicate that their chemical shifts for carbon resonances resonate at almost same frequency.

Table S2.3 Signals originating from chlorosomes in INEPT spectra

Position	Chemical shift (ppm)
F10-CH	124.0
F1-CH_2	60.8
17-CH	49.4
18-CH	47.7

F4-CH_2	39.4
17^2-CH_2	31.7
17^1-CH_2	29.9
F5-CH_2	26.2
3^2-CH_2	22.1
8^1-CH_2	19.1
8^2-CH_3	16.6
$F3^1$-CH_3	15.6
2^1-CH_3	13.7
7^1-CH_3	10.8

Table S2.4 2-D experimental parameters

Experiment	Dipolar 2-D hCH[3,4]
ns	32
ds	8
d1(s)	1.2
^{1}H 90º (kHz)	105
^{13}C 90º (kHz)	51
^{1}H 90º (kHz) Back CP	114
^{13}C 90º (kHz) Back CP	44.25
^{1}H dec (kHz)	15
^{13}C dec (kHz)	15
Water suppression (kHz)	17
Mississippi[5]	
MAS	60
Set T	245
Decoupling	PISSARRO[6]

List of abbreviations:

ns	Number of scans
ds	dummy scans
$^{1}H/^{13}C$ 90º	hard 90º pulses applied on both channels
$^{1}H/^{13}C$ dec	applied on both channels during decoupling
MAS	Magic Angle Spinning rate
Set T	set Temperature
d1	recycle delay

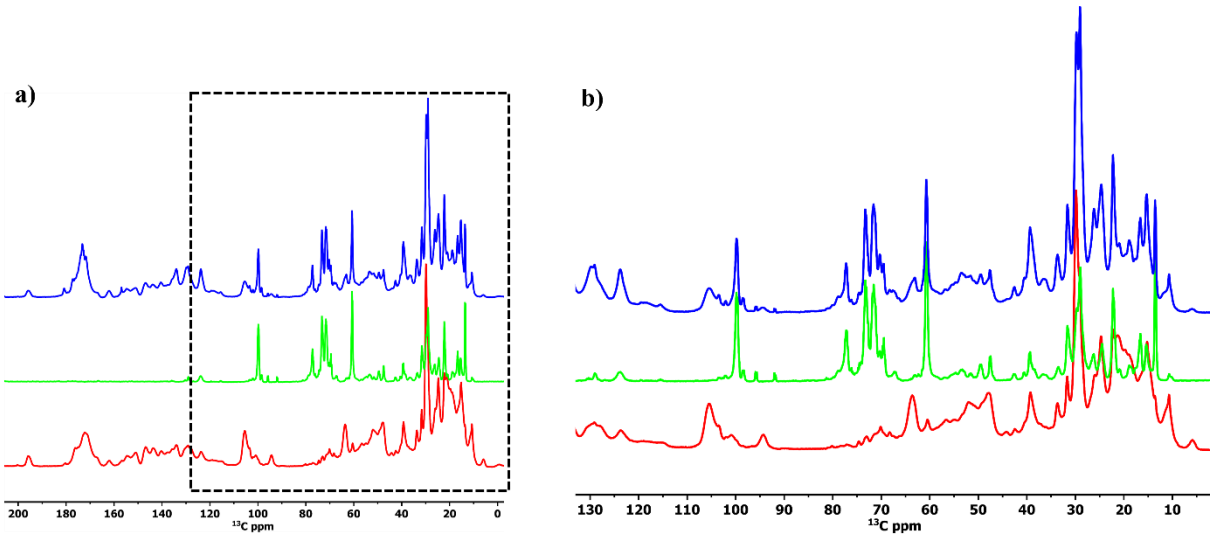

Figure S2.1 a) Overlaid CP (Red), DP(Blue) and INEPT(Green) spectra of chlorosomes of *bchQ* at 277K spinning at 20kHz. b) Enlarged image in the boxed area of a).

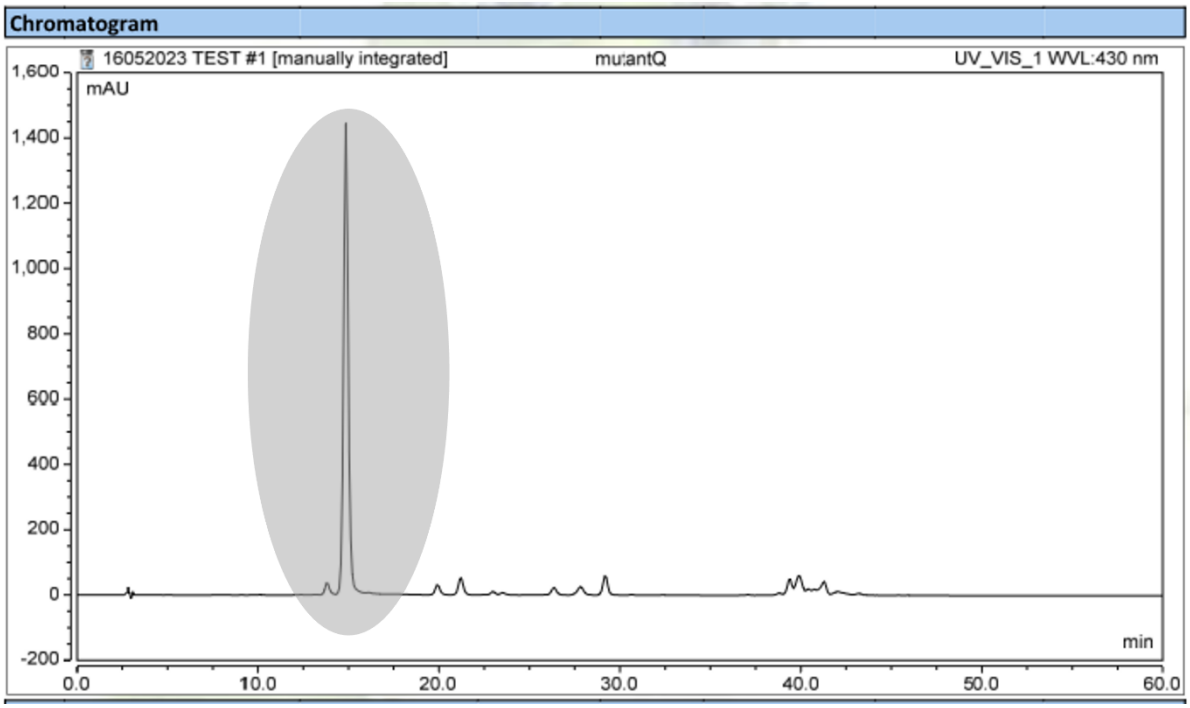

Figure S2.2 Chromatogram of *bchQ,* which shows 2 signals between 10-20 minutes, highlighted in grey. The smaller peak corresponds to 5% [Me, Et] and the larger peak corresponds to 95%[Et, Et]

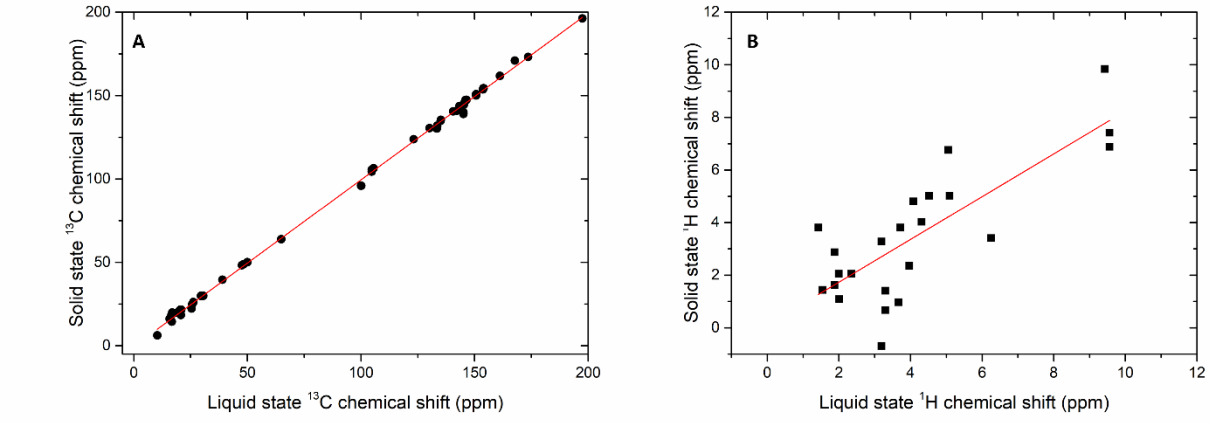

Figure S2.3 Chemical shift correlation plots of *bchQ* chlorosomes. The ^{13}C and ^{1}H shifts in the solid-state NMR data are plotted against the monomer shifts in the solution-state NMR data. The solid line represents the diagonal. The filled circles and squares representing ^{13}C and ^{1}H, respectively, deviating from the solid line correspond to the aggregation shifts due to neighboring BChl molecules.

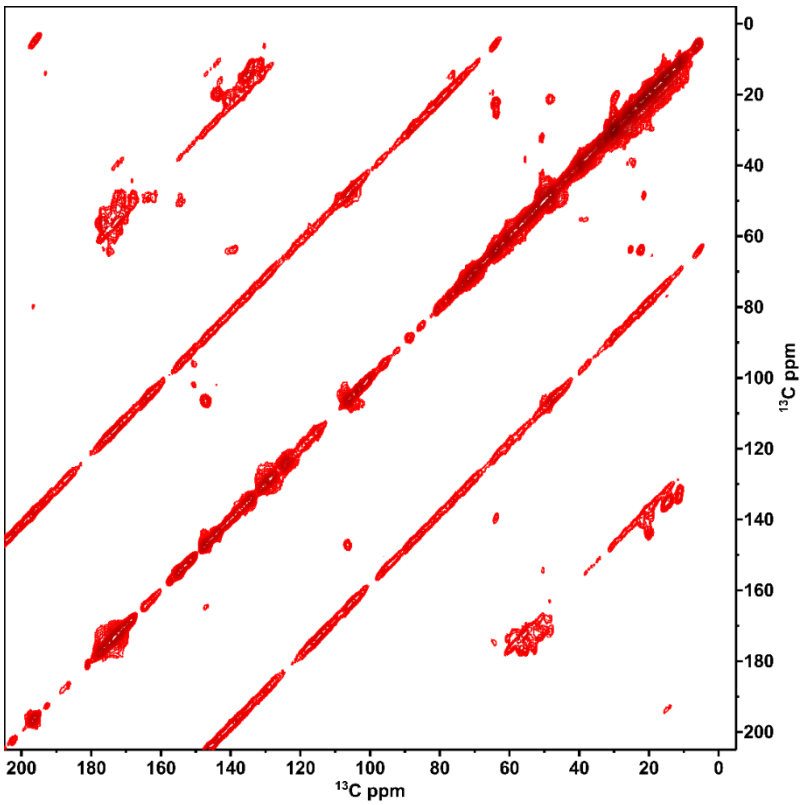

Figure S2.4 ^{13}C-^{13}C RFDR spectra of *bchQ* recorded at 277K, 11kHz, 3.2 ms mixing time. The spectra show short-range intramolecular correlations.

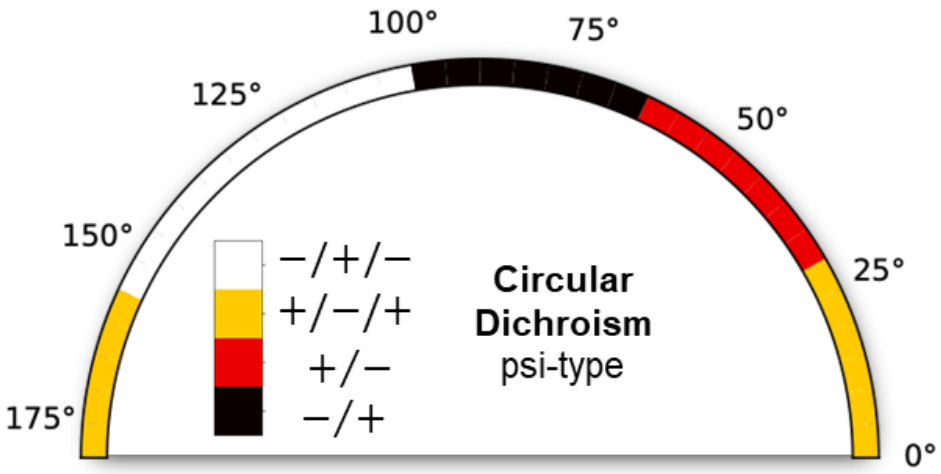

Figure S2.5 Polar plot of spectral features for CD as a function of chiral angle δ. The resolution for δ is 5º. The figure is drawn according to Li *et al*, taking into account the reversed signs in the direction of opposite curvature.[7]

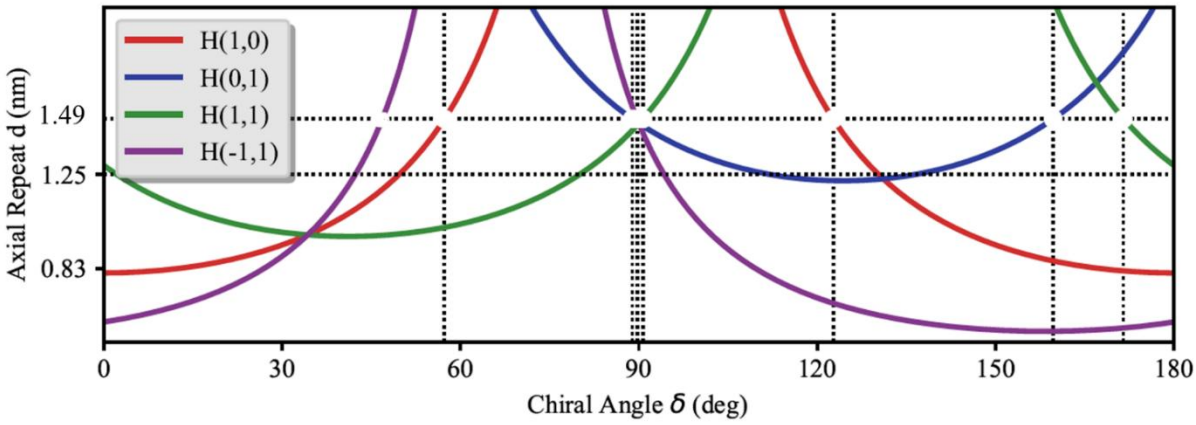

Figure S2.6 The axial repeat d as a function of the chiral angle δ ϵ [0, 180] corresponds to the H(1, 0), H(0, 1), H(1, 1) and H(-1, 1) helical families. Since we are targeting the experimentally determined axial repeat distance d-1.49 nm for *bchQ*, an additional dotted line was drawn. The lattice parameters are set to (1.48, 0.98, 124.3º) as determined from MD simulations of BChl *c* tubular assemblies to evaluate the geometrical relations. Matching chiral angles are highlighted by white circles.

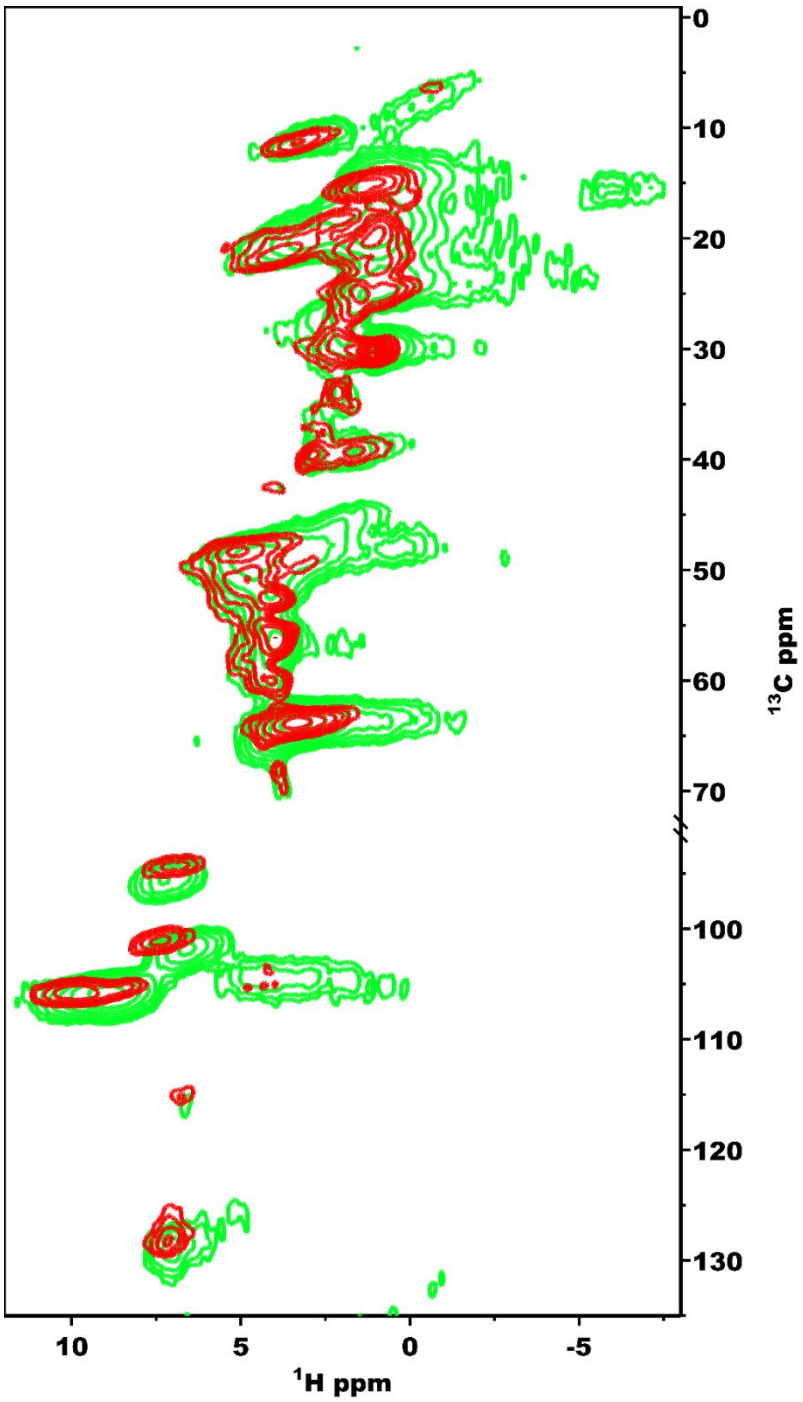

Figure S2.7 is a dipolar hCH spectra of WT (Green) and *bchQ* (Red), recorded in a 1.2 GHz magnet spinning at 60 kHz. The cross peaks for the *bchQ* are well resolved in comparison to WT, revealing the heterogeneity of chlorosomes of the WT

References

(1) Balaban, T. S.; Holzwarth, A. R.; Schaffner, K.; Boender, G.-J.; de Groot, H. J. M. CP-MAS 13C-NMR Dipolar Correlation Spectroscopy of 13C-Enriched Chlorosomes and Isolated Bacteriochlorophyll c Aggregates of Chlorobium Tepidum: The Self-Organization of Pigments Is the Main Structural Feature of Chlorosomes. *Biochemistry* **1995**, *34* (46), 15259–15266. https://doi.org/10.1021/bi00046a034.

(2) van Rossum, B.-J.; Steensgaard, D. B.; Mulder, F. M.; Boender, G. J.; Schaffner, K.; Holzwarth, A. R.; de Groot, H. J. M. A Refined Model of the Chlorosomal Antennae of the Green Bacterium *Chlorobium Tepidum* from Proton Chemical Shift Constraints Obtained with High-Field 2-D and 3-D MAS NMR Dipolar Correlation Spectroscopy. *Biochemistry* **2001**, *40* (6), 1587–1595. https://doi.org/10.1021/bi0017529.

(3) Paulson, E. K.; Morcombe, C. R.; Gaponenko, V.; Dancheck, B.; Byrd, R. A.; Zilm, K. W. High-Sensitivity Observation of Dipolar Exchange and NOEs between Exchangeable Protons in Proteins by 3D Solid-State NMR Spectroscopy. *J. Am. Chem. Soc.* **2003**, *125* (47), 14222–14223. https://doi.org/10.1021/ja037559u.

(4) Barbet-Massin, E.; Pell, A. J.; Retel, J. S.; Andreas, L. B.; Jaudzems, K.; Franks, W. T.; Nieuwkoop, A. J.; Hiller, M.; Higman, V.; Guerry, P.; Bertarello, A.; Knight, M. J.; Felletti, M.; Le Marchand, T.; Kotelovica, S.; Akopjana, I.; Tars, K.; Stoppini, M.; Bellotti, V.; Bolognesi, M.; Ricagno, S.; Chou, J. J.; Griffin, R. G.; Oschkinat, H.; Lesage, A.; Emsley, L.; Herrmann, T.; Pintacuda, G. Rapid Proton-Detected NMR Assignment for Proteins with Fast Magic Angle Spinning. *J. Am. Chem. Soc.* **2014**, *136* (35), 12489–12497. https://doi.org/10.1021/ja507382j.

(5) Zhou, D. H.; Rienstra, C. M. High-Performance Solvent Suppression for Proton-Detected Solid-State NMR. *J. Magn. Reson. San Diego Calif 1997* **2008**, *192* (1), 167–172. https://doi.org/10.1016/j.jmr.2008.01.012.

(6) Weingarth, M.; Tekely, P.; Bodenhausen, G. Efficient Heteronuclear Decoupling by Quenching Rotary Resonance in Solid-State NMR. *Chem. Phys. Lett.* **2008**, *466* (4–6), 247–251. https://doi.org/10.1016/j.cplett.2008.10.041.

(7) Li, X.; Buda, F.; De Groot, H. J. M.; Sevink, G. J. A. The Role of Chirality and Plastic Crystallinity in the Optical and Mechanical Properties of Chlorosomes. *iScience* **2022**, *25* (1), 103618. https://doi.org/10.1016/j.isci.2021.103618.

Appendix 2 Supporting Information for Chapter 3

The Conformational Dynamics of Bacteriochlorophyll *c* in Chlorosomes from the *bchQ* Mutant of *Chlorobaculum tepidum*

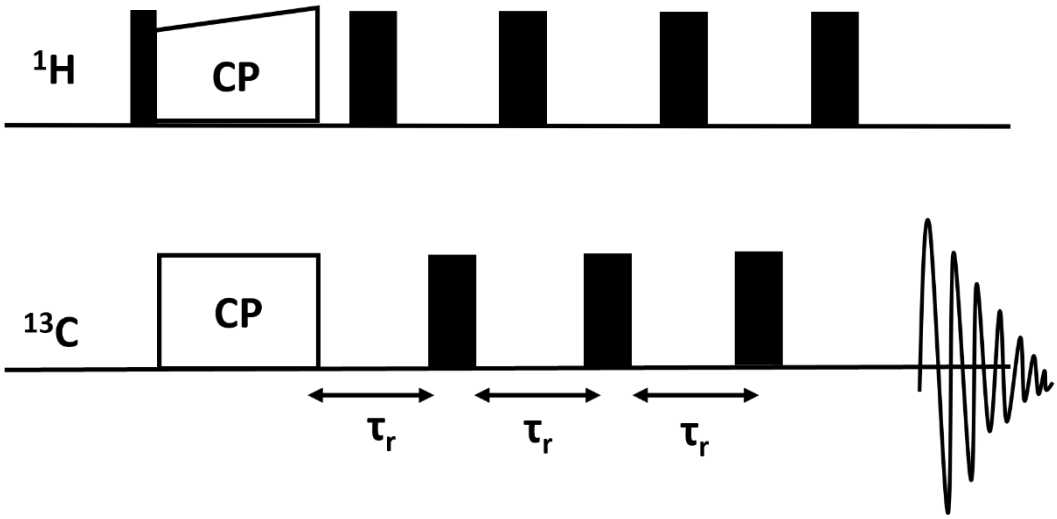

Figure S3.1 pulse sequence used for ^{13}C {^{1}H} REDOR NMR.^{13}C is used as the observe channel and refocusing π pulses are applied on the ^{1}H channel. The ^{1}H π/2 pulse is 1.5 μs and the CP contact time is set to 2 ms. ^{13}C π pulse is set to 10 μs. The pulse sequence used has been implemented according to Cui *et al*.[1]

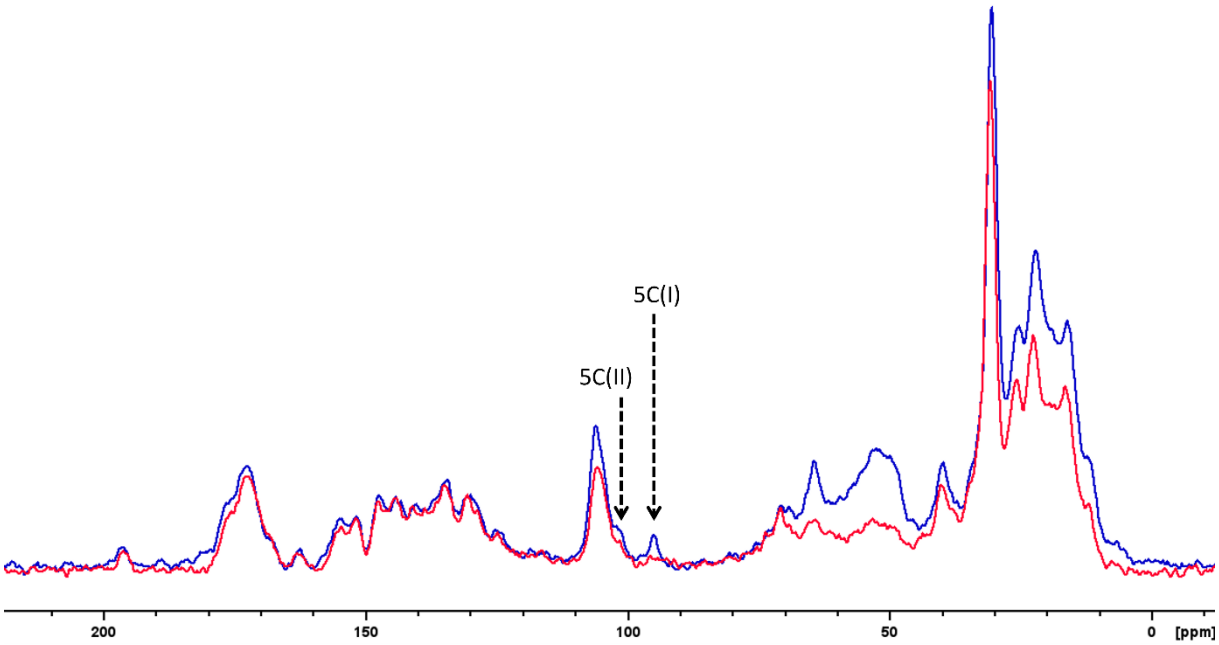

Figure S3.2 $^{13}C\{^{1}H\}$ REDOR S_0 (blue) and S_R (red) spectra of *bchQ* chlorosomes measured at 288 K spinning at 50 kHz in a 1.3 mm rotor. The two dashed arrows indicate the two conformations that are observed in 1-D spectra for the 5C position. The analysis of the REDOR curve mentioned in the main text is performed for the 5C(I) signal which represents ~ 70% of the total signal intensity for both components. The 5C(II) signal overlaps with the peak corresponding to 10, 15, and 20 carbon positions and REDOR works best for isolated spin systems. Therefore 5C(I) was chosen for the analysis. From the S_0 and S_R spectra, the dephasing ratios S_R/S_0 for the carbonyl (CO), methyl (CH_3) and methine (CH) groups in the above spectra are also comparable to the dephasing ratios of 90 %, 47 % and 8 % for the CO, CH_3 and CH groups observed for L valine by Ishii *et al.*[2]

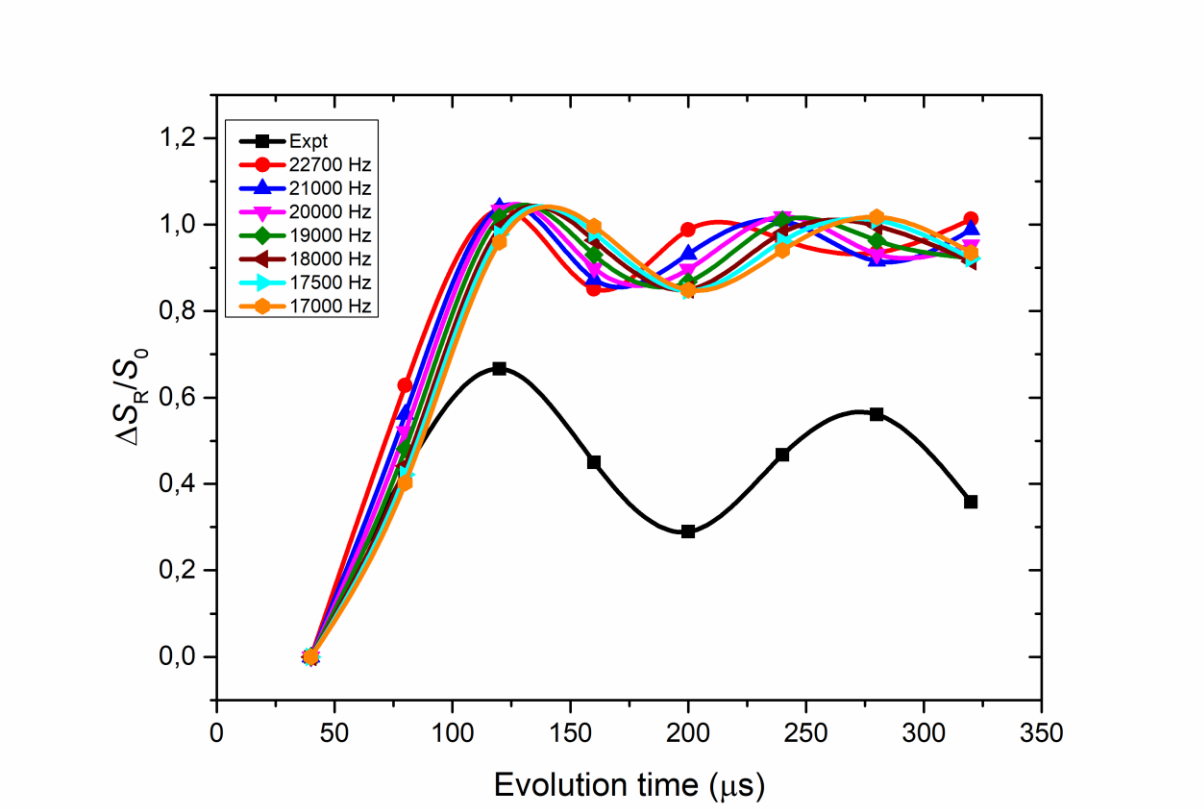

Figure S3.3 $^{13}C\{^{1}H\}$ dephasing curve as a function of time. The Black cubic spline represents the experimentally obtained data set. The colored dephasing curves were obtained by simulation using SIMPSON for different distances. The best match of the dipolar coupling strength to the experimental dephasing frequency is found for a dipolar coupling strength of 17.5 kHz, based on the first minimum and the second maximum of the dephasing curve (Cyan spline).

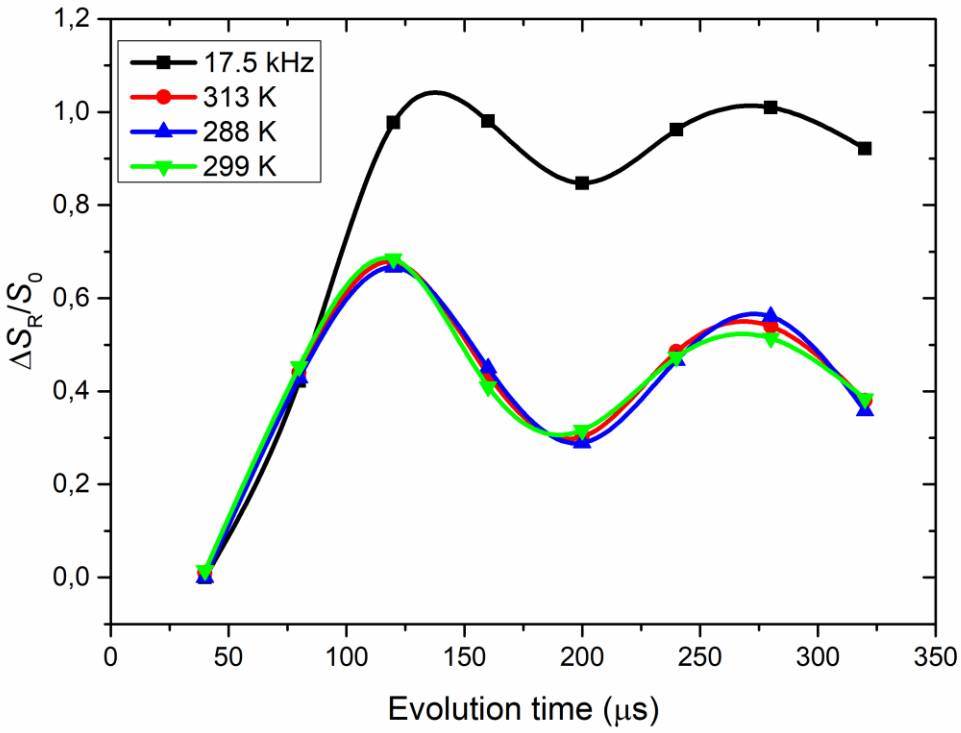

Figure S3.4 REDOR $^{13}C\{^{1}H\}$ dephasing curve as a function of time at 288 K, 299 K, and 313 K and its close match with the dipolar coupling strength obtained from SIMPSON[3] simulation for 17.5 kHz.

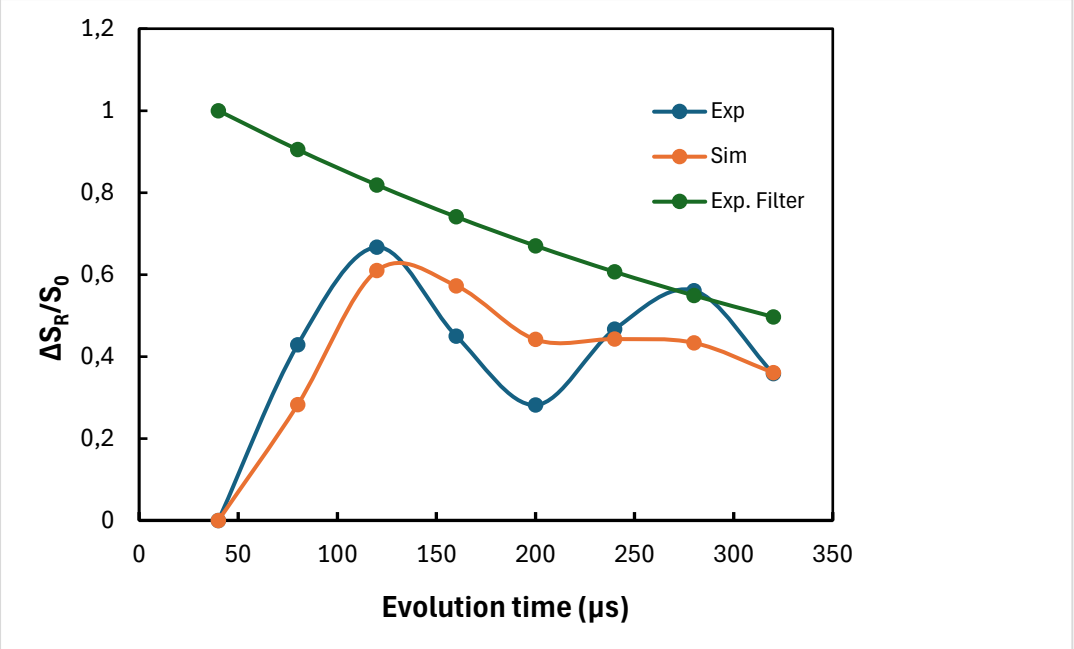

Figure S3.5 Best fit of the model data $m(t_i)$ for a coupling strength of 17500 Hz to the experimental REDOR $^{13}C\{^1H\}$ dephasing data set $d(t_i)$. As before, we employ a cubic spline interpolation for visualisation purposes. In addition to a time-independent scaling factor c, we have introduced a time-dependent exponentially decaying filter exp(-t/a) and minimized $res(t_i)=d(t_i)-c*exp(-t/a)*m(t_i)$ for both c and a, and in the least squares sense. The best fit was determined for a=400 **µ**s and c=0.775, with a RMSD of 0.0970. Applying the same procedure for model data for coupling strengths of 17 kHz and 18 kHz provides c=0.776 and RMSD=0.1014 and c=0.772 and RMSD=0.0939, respectively. We note that the same exponential filter was determined optimal for these values.

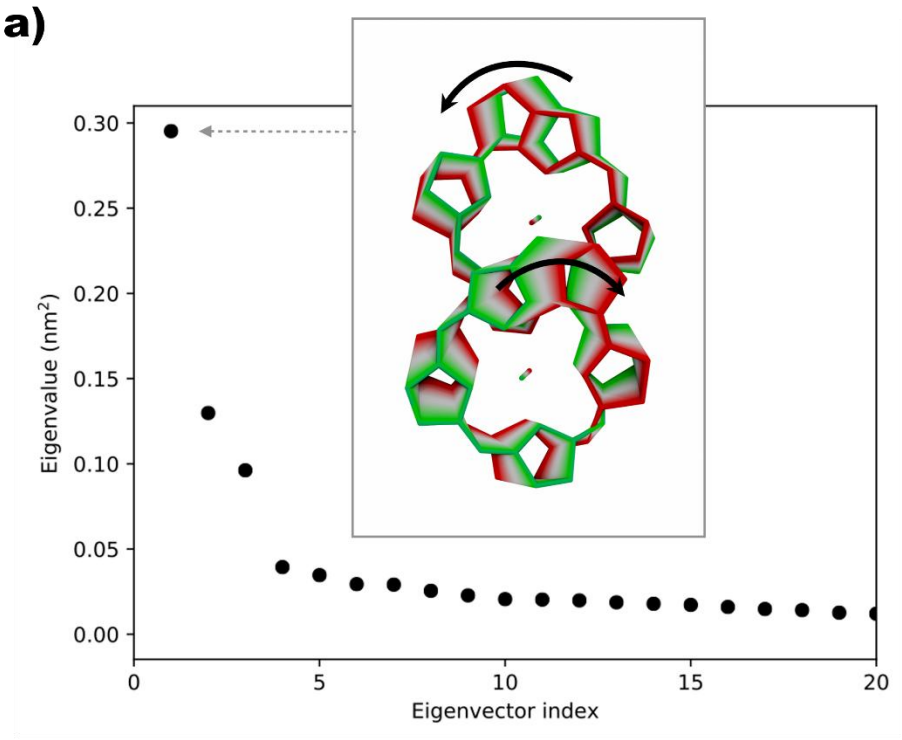

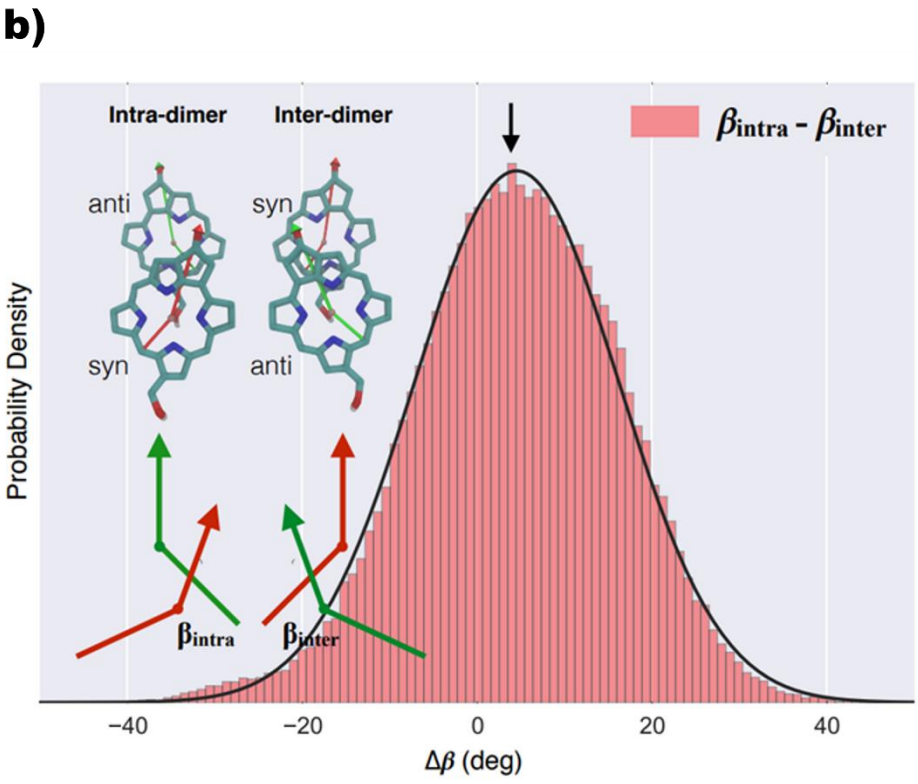

Figure S3.6 a) Principal component analysis (PCA) results for a dimer trajectory that was randomly selected from a tube at T=300 K. The notion of chlorosomes as a plastic molecular crystal or rotator phase is based on the observation of persistent, dominant rotational (or librational) motion exhibited by the BChl macrocycle. The graph shows the magnitude of the

eigenvalue plotted against the eigenvector index. Additionally, the inset displays the first mode, with arrows indicating the rotational directions and green representing earlier and red later stages, respectively. Only a few modes are identified as significant based on the magnitude of the eigenvalues. The primary rotational motion perturbs the hydrogen bonding network, as the rotation can either break or form hydrogen bonds between moieties in neighboring macrocycles.[5] The other modes correspond to experimentally observed side chain fluctuations and tail dynamics described in the main text. Figure reproduced from Li *et al*.[4] Copyright (2022) Elsevier.

b) The *syn-anti* dimer is the structural unit of the stack, with the orientations between *syn-anti* and anti-syn pairs alternating along the stacking direction. The distribution of the relative angle, i.e. the difference $\beta_{intra} - \beta_{inter}$ between neighboring intradimer and interdimer rotation angles, see the inset for a definition of β_{intra} and β_{inter}, is due to dynamic heterogeneity and was extracted from an MD trajectory for a (30, 30) BChl *c* system simulated at a temperature of 300 K.

The important part of the sampling distribution obtained from relatively short molecular simulation between 500 ps and 1 ns lies between -20º to 20º around the average value, spanning about 40º in total, a value that is in very good agreement with the effective θ=48º ±4º angle obtained from the two-site model. Figure 8 of Li *et al*,[5] showing the relative angle distribution at a much lower temperature of 50 K, illustrates the persistence of the dynamics towards low temperatures. While the distribution width is conserved at T=50 K compared to T=300 K, the bimodal nature of the angle distribution signals an undersampling in the considered 500 ps to 1 ns interval due to a weaker thermal driving force, which will not be observed on the timescale of NMR. Figure reproduced from Li *et al*.[5] Copyright (2018) American Chemical Society.

REDOR script used for simulations

```
spinsys {
  channels 1H 13C
  nuclei   1H 13C
  dipole 1 2 -17500 0 98.58 -25.11

}

par {
variable index          1
np                      8
spin_rate                       50000
proton_frequency        750e6
start_operator          I2x
detect_operator         I2p
method                   direct
crystal_file             rep320
gamma_angles             32
sw                      spin_rate/2
variable tsw            1e6/sw
verbose                 1101
variable tr             1e6/spin_rate
variable tr2             0.5e6/spin_rate
variable rf             166000
variable t180           0.5e6/rf
}

proc pulseq {} {
global par

set t180 [expr 0.5e6/$par(rf)]
set tr2 [expr 0.5e6/$par(spin_rate)-$t180]
reset
delay $tr2
```

```
pulse $t180 0 x $par(rf) x
delay $tr2
pulse $t180 0 x $par(rf) y
store 1
reset
acq
delay $tr2
pulse $t180 0 x $par(rf) y
delay $tr2
pulse $t180 $par(rf) x 0 x
prop 1
store 2
acq
for {set i 2} {$i < $par(np)} {incr i} {
reset
prop 1
prop 2
prop 1
  store 2
  acq
}
}


proc main {} {
  global par

  set f [fsimpson]
  fsave $f $par(name),$par(index).fid
}
```

References

(1) Cui, J.; Olmsted, D. L.; Mehta, A. K.; Asta, M.; Hayes, S. E. NMR Crystallography: Evaluation of Hydrogen Positions in Hydromagnesite by 13C1H REDOR Solid-State NMR and Density Functional Theory Calculation of Chemical Shielding Tensors. *Angewandte Chemie International Edition* **2019**, *58* (13), 4210–4216. https://doi.org/10.1002/anie.201813306.

(2) Ishii, Y.; Wickramasinghe, N. P.; Chimon, S. A New Approach in 1D and 2D 13C High-Resolution Solid-State NMR Spectroscopy of Paramagnetic Organometallic Complexes by Very Fast Magic-Angle Spinning. *J. Am. Chem. Soc.* **2003**, *125* (12), 3438–3439. https://doi.org/10.1021/ja0291742.

(3) Bak, M.; Rasmussen, J. T.; Nielsen, N. C. SIMPSON: A General Simulation Program for Solid-State NMR Spectroscopy. *Journal of Magnetic Resonance* **2000**, *147* (2), 296–330. https://doi.org/10.1006/jmre.2000.2179.

(4) Li, X.; Buda, F.; De Groot, H. J. M.; Sevink, G. J. A. The Role of Chirality and Plastic Crystallinity in the Optical and Mechanical Properties of Chlorosomes. *iScience* **2022**, *25* (1), 103618. https://doi.org/10.1016/j.isci.2021.103618.

(5) Li, X.; Buda, F.; de Groot, H. J. M.; Sevink, G. J. A. Contrasting Modes of Self-Assembly and Hydrogen-Bonding Heterogeneity in Chlorosomes of Chlorobaculum Tepidum. *J. Phys. Chem. C* **2018**, *122* (26), 14877–14888. https://doi.org/10.1021/acs.jpcc.8b01790.

Appendix 3 Supporting Information for Chapter 4

MAS NMR Evidence for Plastic Crystallinity of Chlorosomes of the Wildtype *Chlorobaculum tepidum*

Tables

Table S4.1 summarizes the solid-state ^{13}C chemical shifts measured at four different temperatures as observed in the PDSD dipolar based datasets. The splitting into major and minor components for the C5 and C7[1] remains in the approximate 7:3 ratio. All chemical shifts were comparable to the values reported in the literature.[1,2,3]

^{13}C position	296 K	282 K	260 K	230 K
1	154.06	154.64	154.33	153.66
	154.89*	154.79*	154.46*	153.55*
2	135.81	136.44	136.68	136.66
	134.99	134.92	134.91	134.79
2[1]	13.84	15.30	16.52	16.77
	14.33	14.57	14.33	14.57
	13.59	14.33	14.08	14.08,14.33
3	140.39	140.30	139.89	139.75
3[1]	63.73	63.82	63.07	63.30
	62.67	63.40	63.16	63.16
	63.40	63.40	63.40	63.40
	62.92	63.16	62.67	62.67
	64.11	64.09	63.50	63.36
3[2]	26.36	27.03	25.25	25.39
	25.05	24.25	23.78	23.91, 23.12
	22.38	22.87	22.87	
4	144.17	144.41	-	-
	144.19	144.57	144.25	144.16
	144.51	144.62	144.17	143.59

5	101.50	101.74	101.74	101.74
	96.12	96.61	96.37	96.61
		96.12		96.37
6	149.73	149.70	149.74	149.61
	150.62	150.18	149.74	149.71
7	133.22	133.51	132.95	132.76
	132.27	132.26	131.86	131.69
7^1	10.91	11.40	11.40	11.56
	7.25	7.49	7.49	7.49
8	141.03	140.76	140.54	140.03
	142.70	142.87	141.95	141.99
8^1	17.75**	17.99**	17.99**	17.99**
	15.06**	15.55**	15.06**	15.06**
	16.04**	16.77**	16.04**	17.50**
8^2	17.75**	17.99**	17.99**	17.99**
	15.06**	15.55**	15.06**	15.06**
	16.04**	16.77**	16.04**	17.50**
9	146.56	147.32	147.07	147.17
	147.32	147.17	147.07	146.56
10	105.65	105.65	105.65	105.65
11	147.13	147.38	147.06	146.84
12	139.20	139.10	139.04	137.87
12^1	17.75	17.99	17.99	17.75
12^2		18.23		18.23
13	127.76	127.85	127.15	126.91
13^1	196.98	197.08	197.07	196.78
	196.65	196.58	196.67	196.85
13^2	47.78	48.51	48.51	48.27
	48.27	48.83#	48.27	48.30#
	48.51#		48.65#	48.51
			48.51	
14	163.46	163.54	163.47	163.21

15	104.21#	103.62#	103.23#	103.23#
16	154.44	154.37	154.23	154.30
	154.85	154.48	154.46	153.55
	154.89*	154.79*	154.46*	153.55*
17	51.05	51.23	50.67	50.35
17^{1}	29.22	29.22	29.47	29.71
	28.73	29.47	28.98	29.95
	28.24	31.42	29.47	28.77
	29.71			
17^{2}	30.69	31.66	31.17	30.20
	31.66	32.84	31.66	31.42
17^{3}	173.41	173.40	173.00	172.37
	173.31	173.04	172.80	172.45
	173.52	172.97	172.91	172.60
18	48.75	48.40	47.89	48.18
	48.97	47.89	48.34	
18^{1}	20.68	20.68	20.68	20.68
	20.92*	21.41*	21.16*	21.90*
19	170.16	169.97	170.02	169.29
20	104.18	104.67	104.91	104.18
	105.02	105.36	105.26	104.77
	104.30	104.06	105.14	105.19
	104.67	104.43		104.91
20^{1}	20.19	20.68	20.19	20.68
	20.92*	21.41*	21.16*	21.90*
F1	60.48#	60.23#	60.21#	59.47#
F2	119.08#	119.56#	118.83#	120.54#
F3	141.01	141.39	-	-
$F3^{1}$	15.55	15.79	15.55	15.55
F4	40.14	39.87	39.42	39.82
	38.99	39.48		
F5	26.05***	26.29***	26.05***	25.80***

F6	124.67***	124.62***	124.07***	123.73***
		123.69***	122.19***	
F7	134.88	135.18	135.64	134.92
F7[1]				
F8	39.85	39.86	39.37	39.42
	39.48	39.72	39.48	39.72
	39.23	39.23	39.72	
F9	26.05***	26.29***	26.05***	25.80***
F10	124.67***	124.62***	124.07***	123.73***
		123.69***	122.19***	
F11	130.46	131.09	131.02	130.60
F11[1]	n	n	n	n
F12	n	n	n	n

The ^{13}C numbering is according to the IUPAC scheme (cf. Figure S3.1). While chemical shift did not vary much with the temperature, the intensities of the PDSD signals experiment enhanced strongly with decreasing temperature.

Overlap between spinning side bands and cross peak could not be resolved well.

* Chemical shift values are almost the same.

** Chemical shift values are almost the same.

*** Chemical shift values are almost the same.

[n] Could not be resolved

Figures

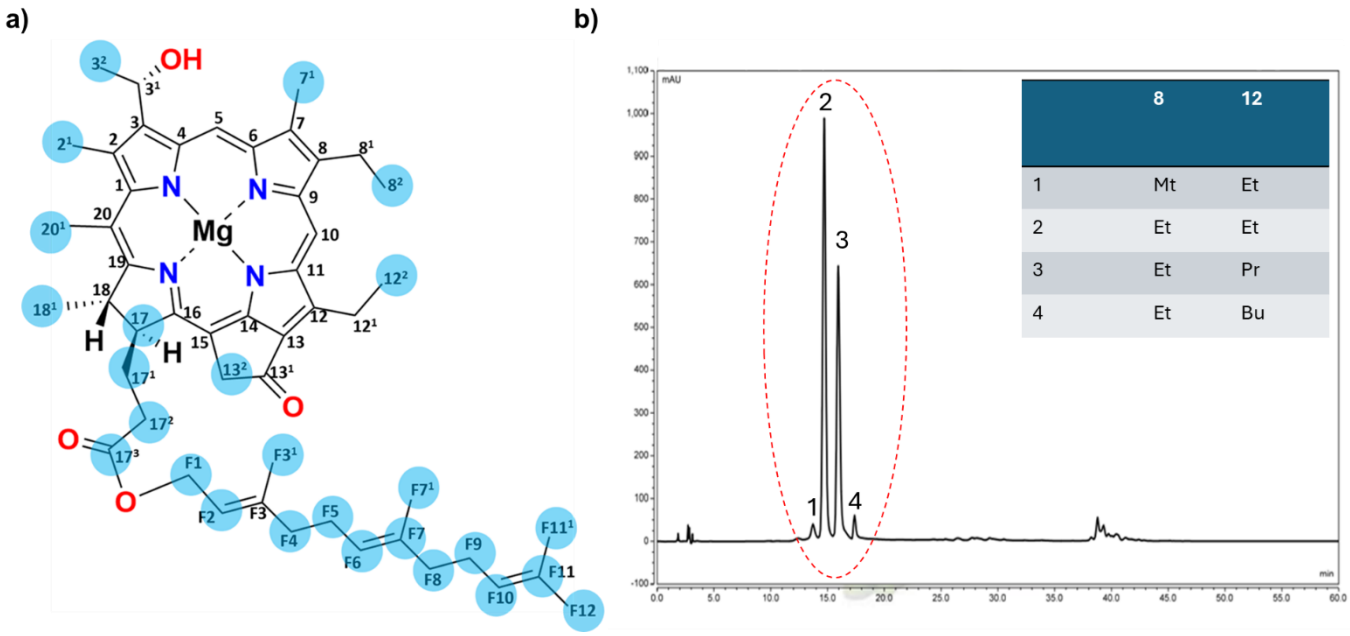

Figure S4.1. a) depicts the chemical structure of BChl *c*, which is the fundamental building block of the tubular chlorosome self-assemblies. Blue spheres indicate dynamic moieties at higher temperatures observed in INEPT, INEPT-TOBSY, and scalar hCH experiments. Additionally, the cross peaks that appeared at lower temperatures in PDSD spectra, which also indicate dynamics, are encircled here. b) displays the chromatogram of WT BChl *c* with four major homologs shown in a table inset. The HPLC technique was performed to assess the distribution of homologs following the established protocols.[2,4] The results align well with the literature.[1–4]

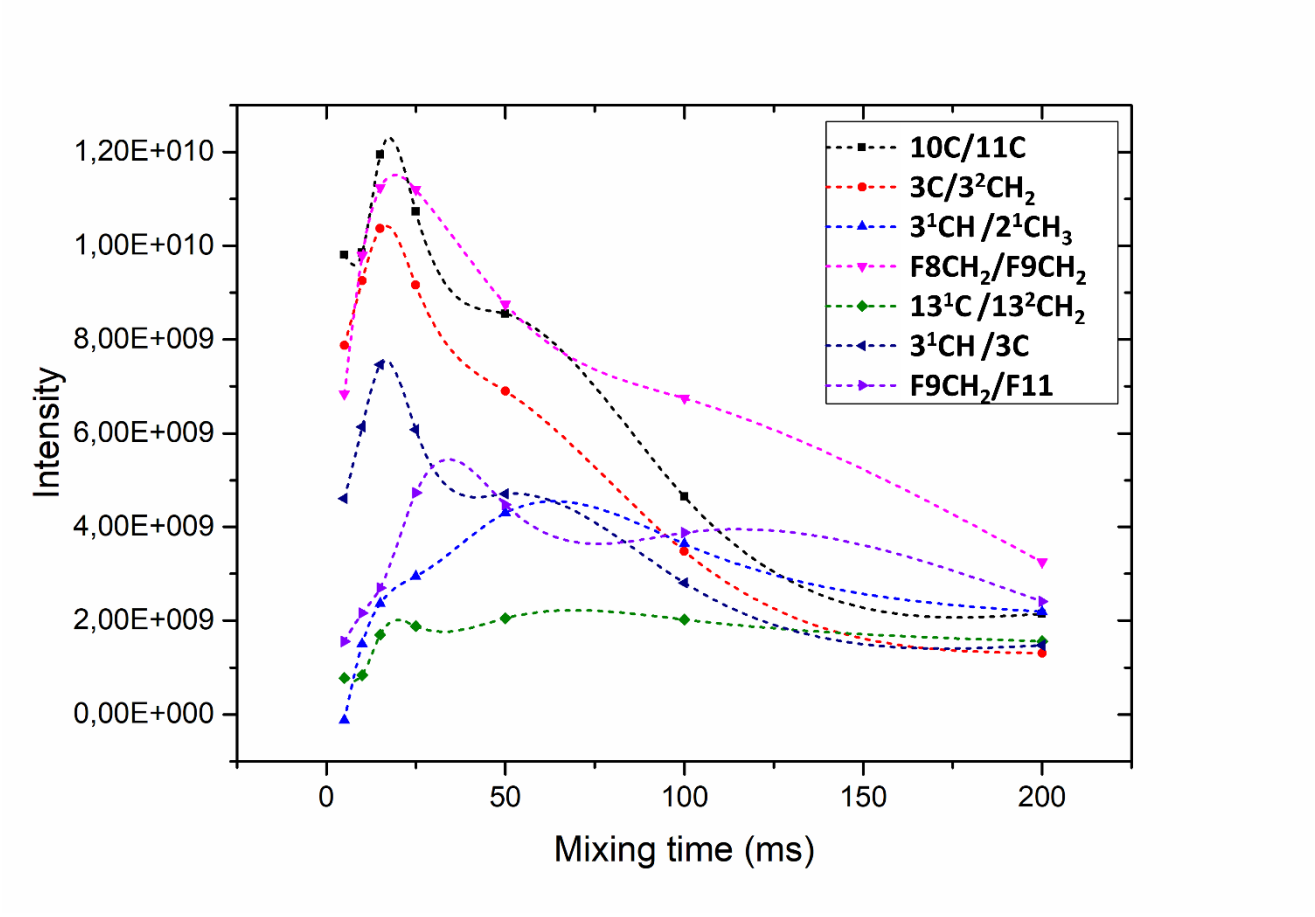

Figure S4.2 shows the build-up curves for several cross peaks detected in the PDSD spectra at 230K. The rate of build-up depends on the strength of the dipolar couplings, and it is affected by local dynamics.

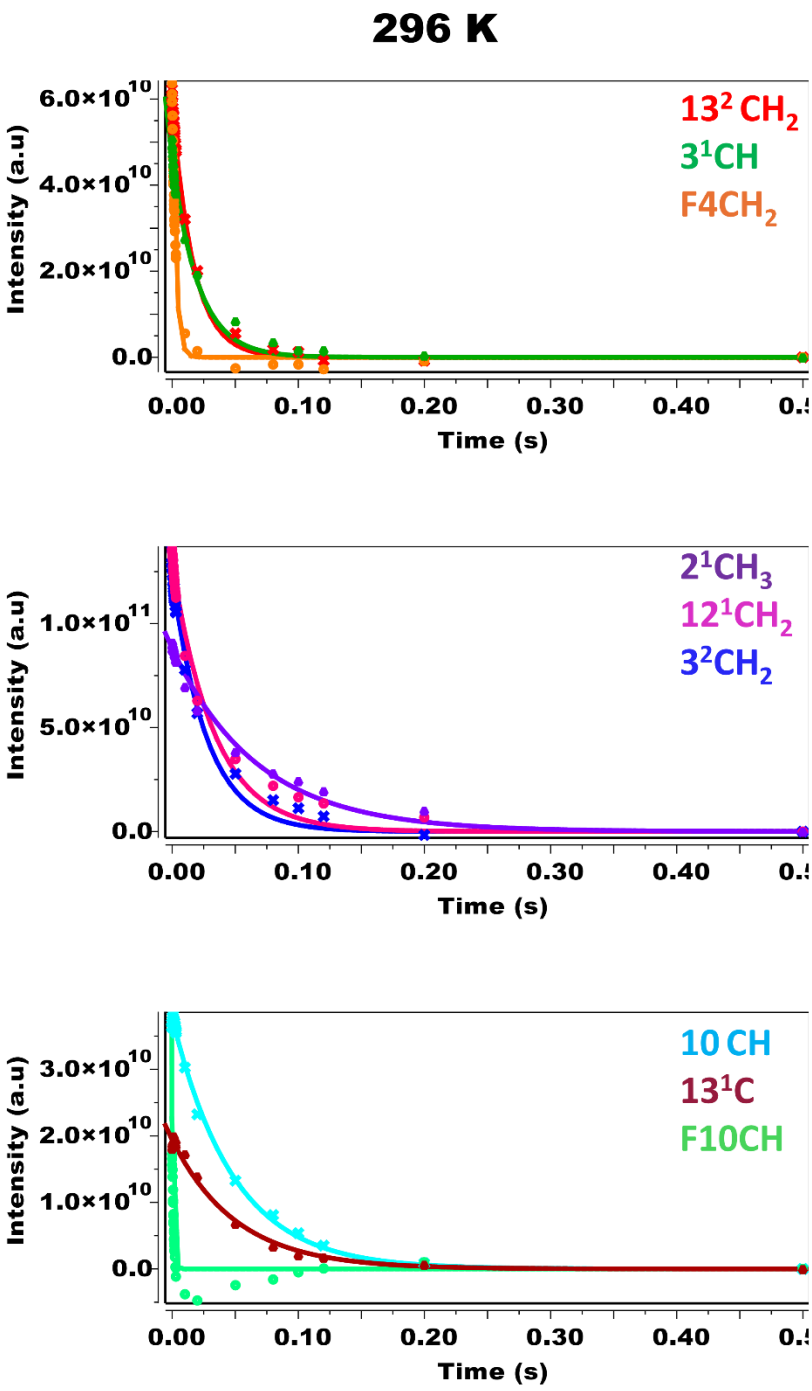

Figure S4.3 shows the ^{13}C $T_{1\rho}$ curves for the WT chlorosomes at 296 K.

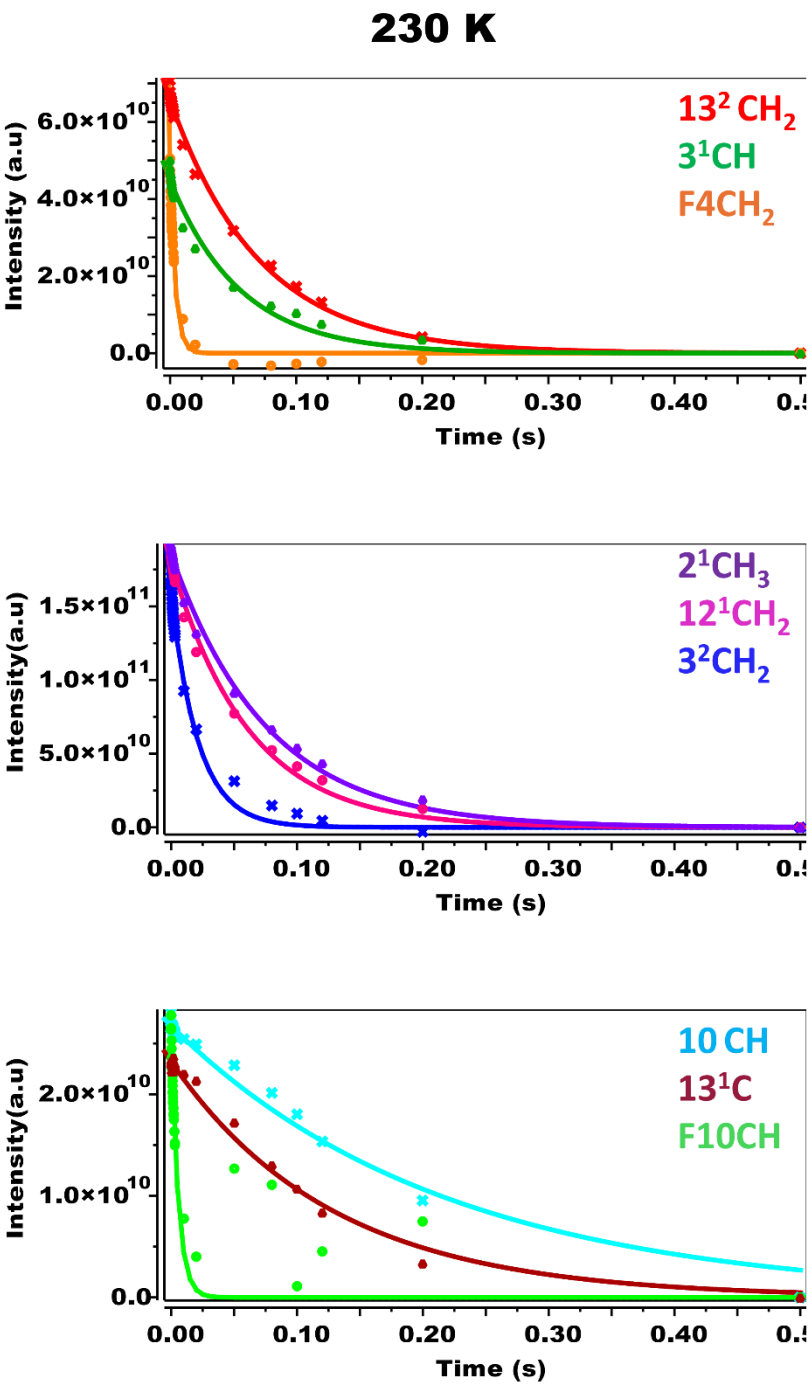

Figure S4.4 shows the ^{13}C $T_{1\rho}$ curves for the WT chlorosomes at 230 K.

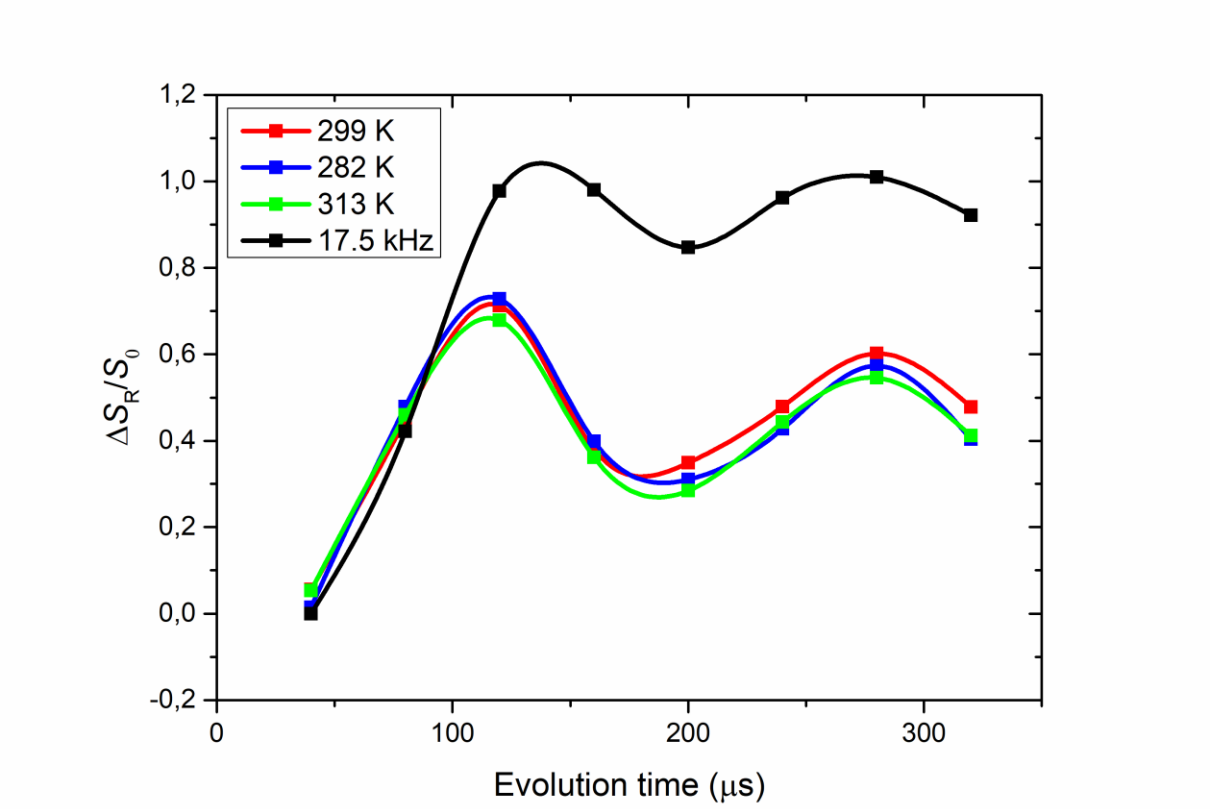

Figure S4.5 shows dipolar dephasing of $^{13}C\{^{1}H\}$ as a function of evolution time at 282 K, 299 K and 313 K. The frequency of oscillations of the experimental curves are in close agreement with the simulated curve for dipolar coupling strength of 17.5 kHz. Simulation was done using SIMPSON.[5]

References

(1) Ganapathy, S.; Oostergetel, G. T.; Reus, M.; Tsukatani, Y.; Gomez Maqueo Chew, A.; Buda, F.; Bryant, D. A.; Holzwarth, A. R.; de Groot, H. J. M. Structural Variability in Wild-Type and *bchQ bchR* Mutant Chlorosomes of the Green Sulfur Bacterium *Chlorobaculum Tepidum*. *Biochemistry* 2012, *51* (22), 4488–4498. https://doi.org/10.1021/bi201817x.

(2) Balaban, T. S.; Holzwarth, A. R.; Schaffner, K.; Boender, G.-J.; de Groot, H. J. M. CP-MAS 13C-NMR Dipolar Correlation Spectroscopy of 13C-Enriched Chlorosomes and Isolated Bacteriochlorophyll c Aggregates of Chlorobium Tepidum: The Self-Organization of Pigments Is the Main Structural Feature of Chlorosomes. *Biochemistry* 1995, *34* (46), 15259–15266. https://doi.org/10.1021/bi00046a034.

(3) Miloslavina, Y. A.; Thomas, B.; Reus, M.; Gupta, K. B. S. S.; Oostergetel, G. T.; Andreas, L. B.; Holzwarth, A. R.; de Groot, H. J. M. Contrasting Packing Modes for Tubular Assemblies in Chlorosomes. *Photosynth. Res.* 2024. https://doi.org/10.1007/s11120-024-01089-3.

(4) Chew, A. G. M.; Frigaard, N.-U.; Bryant, D. A. Bacteriochlorophyllide *c* C-8 ^{2} and C-12 ^{1} Methyltransferases Are Essential for Adaptation to Low Light in *Chlorobaculum Tepidum*. *J. Bacteriol.* 2007, *189* (17), 6176–6184. https://doi.org/10.1128/JB.00519-07.

(5) Bak, M.; Rasmussen, J. T.; Nielsen, N. C. SIMPSON: A General Simulation Program for Solid-State NMR Spectroscopy. *J. Magn. Reson.* 2000, *147* (2), 296–330. https://doi.org/10.1006/jmre.2000.2179.